Front. Mech. Eng. 2020, 15(2): 294–302
https://doi.org/10.1007/s11465-019-0576-4

RESEARCH ARTICLE

Ziyuan LIU, Hang GAO, Dongming GUO

Experimental study on high-efficiency polishing for potassium dihydrogen phosphate (KDP) crystal by using two-phase air–water fluid

© The Author(s) 2020. This article is published with open access at link.springer.com and journal.hep.com.cn

Abstract A high-efficiency polishing approach using two-phase air–water fluid (TAWF) is proposed to avoid surface contamination and solve the inefficiency of previous water-dissolution polishing techniques for potassium dihydrogen phosphate (KDP) crystal. In the proposed method, controllable deliquescence is implemented without any chemical impurity. The product of deliquescence is then removed by a polishing pad to achieve surface planarization. The mechanism underlying TAWF polishing is analyzed, a special device is built to polish the KDP crystal, and the effect of relative humidity (RH) on polishing performance is studied. The relationship between key parameters of polishing and surface planarization is also investigated. Results show that the polishing performance is improved with increasing RH. However, precisely controlling the RH is extremely difficult during TAWF polishing. Controllable deliquescence can easily be disrupted once the RH fluctuates, which therefore needs to be restricted to a low level to avoid its influence on deliquescence rate. The material removal of TAWF polishing is mainly attributed to the synergistic effect of deliquescence and the polishing pad. Excessive polishing pressure and revolution rate remarkably reduce the life of the polishing pad and the surface quality of the KDP crystal. TAWF polishing using IC-1000 and TEC-168S increase the machining efficiency by 150%, and a smooth surface with a root mean square surface roughness of 5.5 nm is obtained.

Keywords potassium dihydrogen phosphate (KDP) crystal, controllable deliquescence, two-phase air–water fluid, high-efficiency polishing, material removal

Received September 17, 2019; accepted October 28, 2019

Ziyuan LIU, Hang GAO (✉), Dongming GUO
Key Laboratory for Precision and Non-Traditional Machining Technology of Ministry of Education, Dalian University of Technology, Dalian 116024, China
E-mails: hanggao4187@126.com; gaohang@dlut.edu.cn

1 Introduction

Potassium dihydrogen phosphate (KDP) crystal was developed in the 1960s and is among the most typical nonlinear optical materials [1]. KDP crystal has been widely applied to various strategic high-tech fields owing to its excellent properties, such as large nonlinear optical coefficient, good optical homogeneity, and high laser-induced damage threshold (LIDT) [2,3]. This material is irreplaceable as a key component of frequency conversion in inertial confinement fusion (ICF) [4,5]. However, the machining efficiency of high-quality KDP crystal has been substantially degraded due to some difficult-to-machine material characteristics (e.g., softness, brittleness, thermal sensitivity, and deliquescence). Thus, the laser intensity in the ICF facility has been severely restricted, leading to a delay in fusion ignition [6,7]. Efficient machining of high-quality KDP crystal has become a technical bottleneck worldwide.

Machining methods, such as single-point diamond turning (SPDT), magnetorheological finishing (MRF), and ion beam figuring (IBF) have been proposed to solve this problem. A smooth surface with a root mean square (RMS) roughness of 1.09 nm has been successfully obtained through SPDT [8]. However, feed rate and cutting depth are strictly restricted to reduce the negative effects of micro-waviness and subsurface damage, leading to low machining efficiency [9–11]. For MRF, special magnetorheological fluids for the KDP crystal have been developed, and a damage-free surface with an RMS roughness of 0.65 nm has been obtained [12]. Nevertheless, the machining efficiency is considerably compromised to avoid the embedding of carbonyl iron powder and

abrasive [13–15]. In IBF, a mirrorlike surface has also been achieved, but the machining efficiency is extremely low owing to material removal on the atomic scale [16]. Moreover, the high temperature gradient generated on the surface of the KDP crystal during the bombardment of ion beam easily leads to the formation of cracks [17,18]. Although the machining quality is good for these methods, the efficiency still cannot meet the requirement of the ICF facility. For poor quality KDP crystal workblank, at least several hours are needed to achieve surface planarization. Therefore, the KDP crystal workblank must be preprocessed by high-efficiency approaches to quickly remove the initial surface damage before using these machining methods.

Our research team proposed a water-dissolution polishing technique [19,20], in which the water concentration is precisely regulated by micro-emulsion fluid consisting of alcohols, surfactant, and deionized water to achieve controllable deliquescence. The product of deliquescence is then removed by the polishing pad to achieve surface planarization [21–23]. Compared with the above methods, the efficiency of machining is improved remarkably with a material removal rate (MRR) of 500 nm/min [24,25]. However, chemical impurities in the micro-emulsion fluid inevitably contaminate the surface of the KDP crystal and subsequently decrease the LIDT. Hence, a high-efficiency polishing approach without surface contamination should be developed to achieve controllable deliquescence by using other catalysts instead of the micro-emulsion fluid.

This paper proposes a high-efficiency polishing approach for the KDP crystal using two-phase air–water fluid (TAWF), in which water flows as a dispersed phase in a continuous air phase. TAWF has been widely applied in many industrial processes, such as steam generators, chemical reactors, and nuclear reactors [26,27]. Controllable deliquescence is implemented by the TAWF without any chemical impurity. The dissolution layer produced by controllable deliquescence is then removed for surface planarization through the mechanical action of the polishing pads. The mechanism of the proposed method (i.e., TAWF polishing) was investigated, and a special device was then built to polish the KDP crystal. The effect of relative humidity (RH) on polishing performance was analyzed to improve the regulation accuracy of the rate of deliquescence. The relationship between key parameters (i.e., polishing pressure, revolution rate, and polishing pad) and surface planarization was also studied. The results indicate that high-efficiency surface planarization could be achieved by employing TAWF polishing, and the KDP crystal can be well preprocessed for subsequent machining.

2 Mechanism of TAWF polishing

Deliquescence rate increases with moisture absorption. Meanwhile, the surface characteristics of the KDP crystal change differently. With a relatively low deliquescence rate, a dissolution layer that could be easily removed by mechanical action is formed by the deliquescence product. As the rate of deliquescence reaches beyond a certain point, corrosion structures appear on the crystal surface, as shown in Fig. 1. The surface quality of the KDP crystal is substantially degraded because of these structures, which should be avoided for surface planarization. Therefore, the amount of absorption of moisture must be precisely regulated to make deliquescence controllable. To this end, a TAWF polishing was developed. Uniform dispersion of liquid water was performed through the two-phase structure of the TAWF. The amount of moisture absorbed by the KDP crystal could be regulated by changing the supply rate of the TAWF, and the controllable deliquescence was thus implemented.

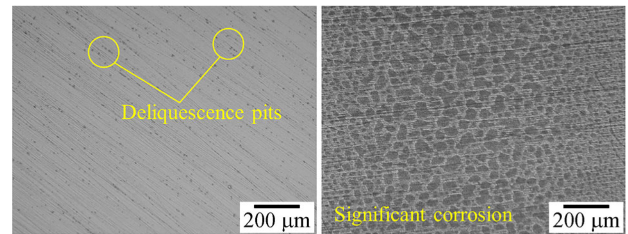

Fig. 1 Corrosion structures of deliquescence.

The mechanism of surface planarization in TAWF polishing is shown in Fig. 2. During the polishing process, discrete water particles in the TAWF located between the polishing pad and the KDP crystal were absorbed to perform controllable deliquescence. A dissolution layer was then formed on the surface of the KDP crystal. The dissolution layer was gradually removed owing to the mechanical action of the polishing pad. However, the MRR of the peaks and valleys of surface micro-topography was different. For the peaks, the dissolution layer could be quickly removed due to the direct contact with the polishing pad. For the valleys, the dissolution layer was located in the recessed region. The mechanical action of the polishing pad was remarkably weakened, which indicates a much lower MRR compared with that of the peaks. Therefore, the distance between the peaks and valleys was reduced, and surface planarization was thus performed. Additionally, owing to the different MRR, the dissolution layer at the valleys could not be fully removed in a timely manner. The residual dissolution layer can inevitably infiltrate into the substrate of the KDP crystal. During the process of infiltration, the dissolution layer absorbs fresh solute from the substrate. A high concentration region is then formed near the surface of the substrate, which impedes the infiltration behavior [28]. Therefore, most of the substrate can be protected.

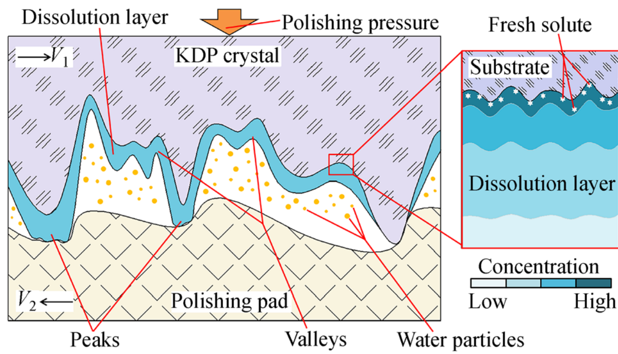

Fig. 2 Surface planarization mechanism in TAWF polishing.

3 Experimental details

3.1 Building a device for TAWF polishing

The TAWF polishing device was mainly composed of six components, namely, TAWF generator, planetary motion system, polishing platform, recovery unit, diffusion chamber, and marble base. A detachable polyethylene (PE) cover and a humidifier were also introduced to regulate RH during the polishing process. The schematic of the TAWF polishing device is shown in Fig. 3. A class 1000 cleanroom, where RH$\leqslant$15% and temperature was 23 °C, was used to place the polishing device.

For the TAWF generator, the uniform dispersion of liquid water was implemented due to the high-frequency vibration of an ultrasonic transducer. Micron-sized water particles were thus formed. Compared with other dispersion techniques, the ultrasonic one has a number of advantages, such as stability of discrete distribution, consistency of particle size, and controllability of flow rate [29]. The air in the cleanroom was sucked into the TAWF generator by a fan and then mixed with the micron-sized water particles. Thus, the TAWF was formed. The supply rate of the TAWF, described by the mass flow of micron-sized water particles (MF_{mwp}), was controlled by regulating the fan speed.

The diffusion chamber was fixed on the marble base. The polishing platform with some circle-distributed holes was installed on the top of the diffusion chamber. A polishing pad was attached to the upper surface of the polishing platform. The polishing pad also contained holes identical to the holes located on the polishing platform. The recovery unit used to recycle excessive TAWF by creating negative pressure was installed on the edge of the polishing platform. The planetary motion system containing a rotation motor, a revolution motor, and a loading unit was fixed on the marble base. For this motion system, the rates of rotation and revolution can be regulated separately. The loading unit was used to generate the polishing pressure. The KDP crystal was clamped at the bottom of the loading unit.

During the polishing process, the TAWF flowed from the TAWF generator into the diffusion chamber through pipes and then ejected from the holes located on the polishing pad. The KDP crystal executed a planetary motion on the surface of the polishing pad and periodically passed the areas above the holes. The TAWF touched the crystal surface to form a dissolution layer as the KDP crystal reached the area above the hole. Subsequently, the dissolution layer was gradually removed by the polishing pad to achieve surface planarization as the KDP crystal left the area above the hole.

3.2 Preparing for polishing experiments

Polishing experiments were conducted by using the aforementioned polishing device (Fig. 3). KDP crystals

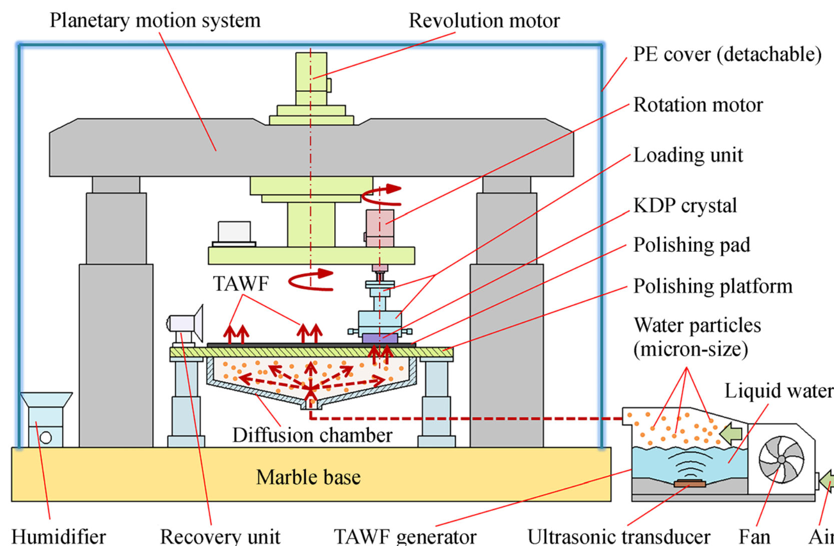

Fig. 3 Schematic of TAWF polishing device.

Table 1 Process parameters of TAWF polishing

Polishing pressure/kPa	Revolution rate/$(\mathrm{r\cdot min^{-1}})$	MF_{mwp} /$(\mathrm{mg\cdot min^{-1}})$	Rotation rate /$(\mathrm{r\cdot min^{-1}})$	Polishing time /min	Preprocessing method	Relative humidity/%
2–20	4–70	150	200	50	Lapping	⩽15

with dimensions of 30 mm× 30 mm× 10 mm were prepared as experimental samples. Fixed abrasive lapping films (Riken Corundum, Japan) were employed in the tests of the effect of RH on polishing performance to preprocess the KDP crystal samples and achieve the consistency of the surface topography with an average RMS surface roughness of 220 nm. A TEC-168S (Chiyoda, Japan) was chosen as the polishing pad. The MF_{mwp} was set to 0 mg/min to highlight the effect of RH. The rate of rotation was set to 230 r/min, the polishing pressure was set to 13 kPa, and the rate of revolution was set at 17 r/min. A temperature humidity meter (Mboos MBS-323, China) was adopted to measure RH. As the precise control of RH is extremely difficult, the fluctuation of RH is inevitable. Therefore, the RH in each test was characterized by average relative humidity (ARH), which was in the range of 15%–90%. The testing time was set to 60 min with regard to each ARH. Furthermore, a series of TAWF polishing experiments were carried out to investigate the effect of key parameters on surface roughness and MRR. The process parameters are listed in Table 1. The polishing pad are: TEC-168S; TEC-6377 (Chiyoda, Japan); 530N7501 (Chiyoda, Japan); and IC-1000 (Dow Chemical, USA).

The surface of the KDP crystal sample was observed by an optical microscope (Olympus MX40, Japan). A 3D surface profiler (Zygo NV5022, USA) was used to obtain the surface profile and RMS surface roughness. An ultra-precision analytical balance (Sartorius CP225D, Germany) was used to calculate the MRR of each polishing experiment. The 3D microcosmic morphologies of the surface and lateral section of polishing pads were detected by a laser scanning confocal microscope (Keyence VK-X200 series, Japan).

4 Results and discussion

4.1 Effect of RH on polishing performance

The RMS surface roughnesses and MRR at different ARHs are shown in Fig. 4. Moisture content was extremely low as ARH was 15%, which was not enough to trigger deliquescence. After 60 min of polishing, the RMS surface roughness was reduced by 4.83% at 214.8 nm, and the MRR was approximately 0 nm/min. Therefore, effective material removal for the KDP crystal without deliquescence could not be performed merely by the polishing pad. The polishing performance was not affected by low ARH

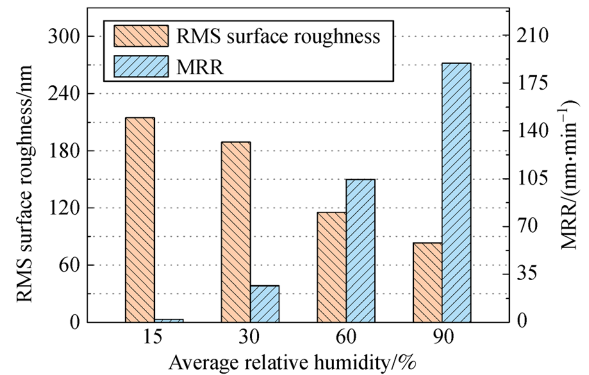

Fig. 4 RMS surface roughnesses and MRR at different ARHs.

(⩽15%) at 23 °C.

Subsequently, as the ARH increased from 15% to 60%, the RMS surface roughness reduced to 115.3 nm, and the MRR rose to 104.5 nm/min. Moisture content increased with the rise in ARH. Meanwhile, deliquescence occurred on the surface of the KDP crystal. The rate of deliquescence rose with rising ARH and subsequently led to an increase in the formation rate of the dissolution layer. As this layer was removed by the polishing pad, the efficiency of surface planarization and MRR rose accordingly. Figure 5 shows the surface topography of the KDP crystal before and after the polishing process at an ARH of 60%. The depth and distribution density of lapping textures, which were mainly composed of parallel scratches, greatly decreased.

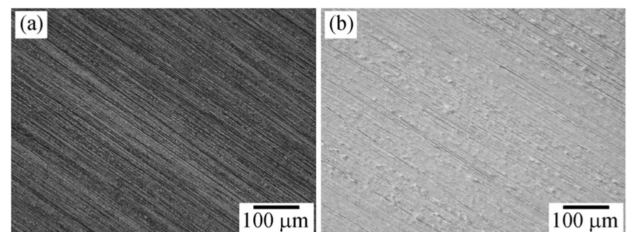

Fig. 5 Surface topography of KDP crystal before and after the polishing process at an ARH of 60%. (a) Before polishing; (b) after polishing.

When the ARH reached 90%, the RMS surface roughness decreased by 63%, and the MRR reached 189.4 nm/min. Hence, improving the polishing performance with increasing RH is theoretically feasible. However, this method has not been successfully implemented yet because

the precise control of RH is extremely difficult during TAWF polishing. Once RH fluctuates, controllable deliquescence can easily be disrupted and lead to the formation of corrosion structures (Fig. 1). Therefore, RH needs to be restricted to a low level to avoid its influence on the deliquescence rate, which is controlled by regulating the supply rate of the TAWF.

Based on the above investigations, material removal in TAWF polishing is mainly contributed by the synergistic effect of deliquescence and the polishing pad. The possible ways of material removal can be expressed as:

$$MR = MR_m + MR_d + MR_s, \quad (1)$$

where MR is the total amount of material removal in TWAF polishing, and MR_m, MR_d, and MR_s are the amount of material removal derived from the mechanical action of the polishing pad, deliquescence, and the synergistic effect of these two factors, respectively. MR_m is approximately 0 g because no effective material removal can be performed merely by the polishing pad. MR_d is always negative because the KDP crystal absorbs moisture in the process of deliquescence. Hence, the majority of MR must be contributed by MR_s.

4.2 Relationship between polishing parameters and surface planarization

The effect of polishing pressure on RMS surface roughness and MRR is shown in Fig. 6. The polishing pad was TEC-168S, and the revolution rate was 13 r/min. As polishing pressure increased from 2 to 8 kPa, MRR became higher, and RMS surface roughness decreased. The mechanical action of the polishing pad was enhanced with the increasing polishing pressure. Consequently, the amount of removal of the dissolution layer rose. Moreover, for the peaks of surface micro-topography, the MRR significantly increased with stronger mechanical action derived from the increasing polishing pressure. By contrast, the valleys located in recessed regions still could not fully come in contact with the polishing pad, thus, MRR was only slightly increased. Hence, the difference of MRR between the peaks and the valleys got larger. The efficiency of surface planarization rose accordingly, an indication of a low RMS surface roughness.

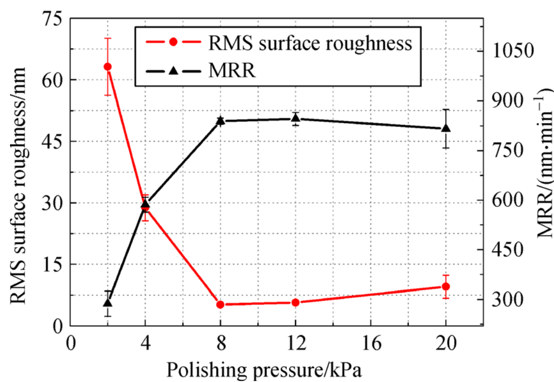

Fig. 6 The effect of polishing pressure on RMS surface roughness and MRR.

The mechanical action of the polishing pad was strengthened when the polishing pressure increased from 8 to 12 kPa. However, MRR and RMS surface roughness remained unchanged (Fig. 6). The formation rate of the dissolution layer was not considered a variable due to a constant MF_{mwp}. The polishing pad touched the substrate without deliquescence as the rate of mechanical action of the polishing pad was higher than that of the formation of the dissolution layer. At this point, no effective material removal can be implemented as evidenced in Section 4.1. Furthermore, RMS surface roughness increased by 67.2% as the polishing pressure increase from 12 to 20 kPa. Meanwhile, a number of black residues were observed on the surface of the KDP crystal (Fig. 7). The abrasion resistance of the TEC-168S was poor owing to the texture of flannelette. The fluff on the TEC-168S was easily worn and shed under excessive polishing pressure. Consequently, the flatness of TEC-168S was reduced, which led to the degradation of polishing performance. Meanwhile, part of the shedding fluff attached to the surface of the KDP crystal to form these black residues.

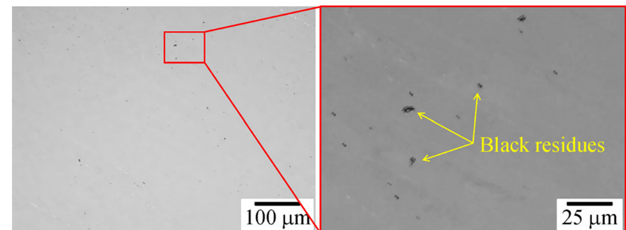

Fig. 7 Black residues on the surface of KDP crystal.

The effect of revolution rate on RMS surface roughness and MRR is shown in Fig. 8. The polishing pressure was 14 kPa, and the polishing pad was TEC-168S. As revolution rate rose from 4 to 16 r/min, the mechanical action of the polishing pad was enhanced, and the removal rate of the dissolution layer became higher. Therefore, the MRR increased. Meanwhile, the difference of MRR between peaks and valleys increased similarly to polishing pressure. Hence, the increased efficiency of surface planarization led to the decrease in RMS surface roughness. When the revolution rate exceeded 16 r/min, the RMS surface roughness began to increase, and the MRR was reduced. The planetary motion of the KDP crystal became unstable, and the stability was reduced with increasing revolution rate. Meanwhile, the close contact between the KDP crystal and the polishing pad was nearly absent, and the efficiency of material removal and surface planarization decreased accordingly. Furthermore, the stability of the planetary motion was significantly reduced

as the revolution rate reached 70 r/min. The polishing pad, which was scratched by the edges of the KDP crystal (Fig. 9), led to a loss of polishing performance.

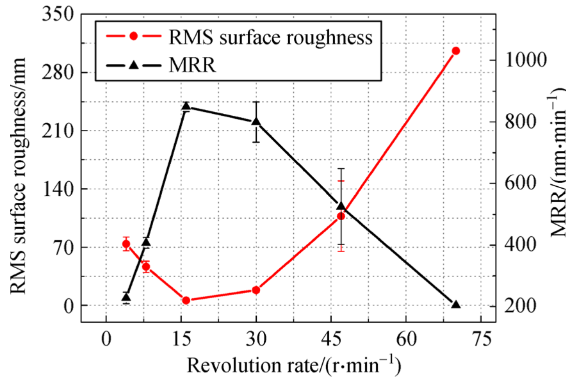

Fig. 8 The effect of revolution rate on RMS surface roughness and MRR.

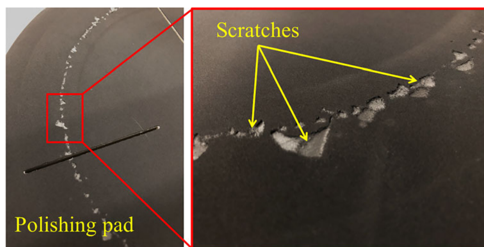

Fig. 9 Scratches on the polishing pad.

4.3 Optimization of polishing pads and its application

Optimization of polishing pads was carried out to further improve the polishing performance. Four kinds of polishing pads (i.e., TEC-6377, IC-1000, 530N7501, and TEC-168S) whose textures were representative were chosen for the polishing tests. The 3D microcosmic morphologies of these polishing pads are shown in Fig. 10. The topographies of corresponding polished surfaces are shown in Fig. 11. For TEC-6377, a large number of scratches derived from the lapping process were not removed, and new scratches were also formed (Fig. 11(a)). TEC-6377 is made of polyurethane and fiber. Part of the fiber is exposed on the surface (Fig. 10(a)). High local pressure was created, under which new scratches easily formed owing to the small contact area between the crystal surface and the exposed fiber. Moreover, the mechanical action of TEC-6377 was substantially degraded due to the smooth surface of the fiber and subsequently decreased MRR.

IC-1000 is mainly made of high-density polyurethane (Fig. 10(b)). The flatness and hardness of IC-1000 were higher than the other three polishing pads. Hence, IC-1000 can avoid the deterioration of flatness of the KDP crystal and improve the efficiency of polishing simultaneously. A high-quality surface could be quickly obtained by using IC-100 as verified through a series of polishing tests (Fig. 11(b)). The corresponding MRR was about 2 μm/min, which increased by more than 400% compared with the previous techniques of water-dissolution polishing [30]. Besides, the machining efficiency of IC-1000 was also much higher than TEC-168S. However, IC-1000 cannot implement a closer contact with the crystal surface owing to low compressibility, which restricted the further improvement of surface quality.

The surfaces of 530N7501 and TEC-168S are made of flannelette (Figs. 10(c) and 10(d)). However, the surface topographies of the KDP crystal obtained by these two polishing pads were different. For the 530N7501, the lapping textures were not completely removed, and the flatness of the crystal surface was bad owing to some uneven regions (Fig. 11(c)). By contrast, a mirrorlike surface was obtained by using TEC-168S (Fig. 11(d)). The

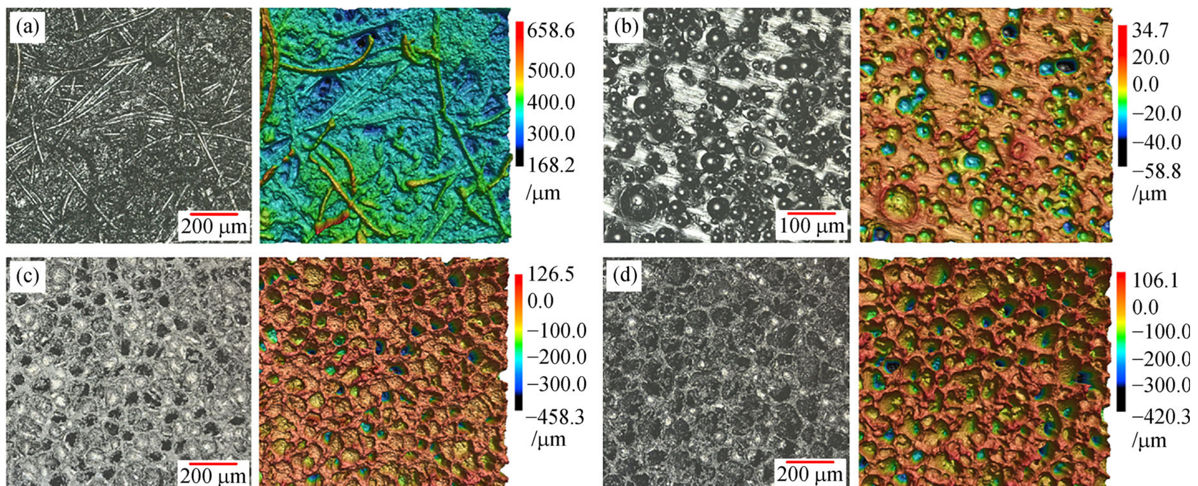

Fig. 10 3D microcosmic morphologies of the polishing pads. (a) TEC-6377; (b) IC-1000; (c) 530N7501; (d) TEC-168S.

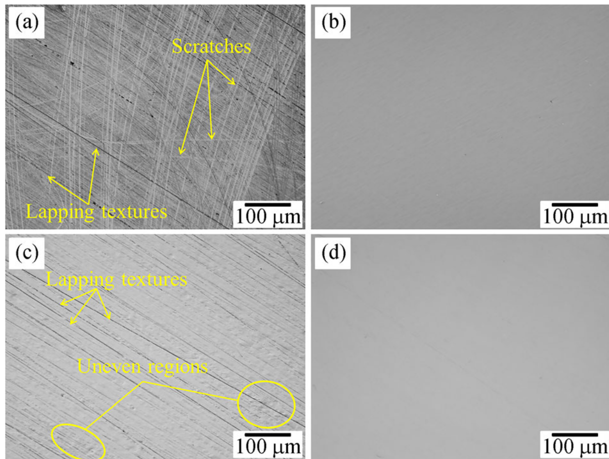

Fig. 11 Surface topographies of KDP crystal obtained by using different polishing pads. (a) TEC-6377; (b) IC-1000; (c) 530N7501; (d) TEC-168S.

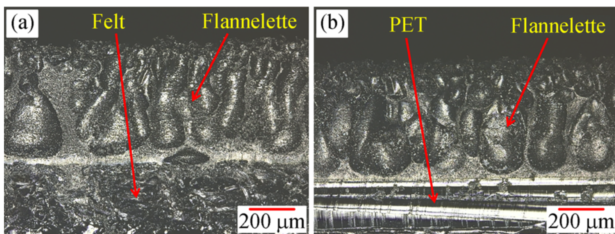

Fig. 12 Microcosmic morphologies of lateral section of the polishing pads. (a) 530N7501; (b) TEC-168S.

main reason for this difference is that the substrates of these two polishing pads were different. The substrate of the 530N7501 was made of felt, which was both soft and resilient (Fig. 12(a)). Excessive local deformations, which were formed during the polishing process to achieve full contact with the surface of the KDP crystal, caused two negative effects. First, the flatness of the KDP crystal was decreased. Second, the mechanical action for the valleys of the surface micro-topography was significantly enhanced. The reduced difference of MRR between the peaks and valleys led to a decreased in the efficiency of surface planarization. The substrate of TEC-168S was synthesized from polyethylene terephthalate (PET) as shown in Fig. 12(b). Excessive local deformation was avoided when TEC-168C was used owing to the high hardness and excellent resistance to deformation of PET.

According to the above studies, a high-efficiency composite process of TAWF polishing was conducted. This process was composed of two polishing stages, and the relevant parameters are listed in Table 2. At the 1st polishing stage, IC-1000 was used to quickly remove the lapping textures and initial damage located on the surface of the KDP crystal. Subsequently, at the 2nd stage of polishing, surface planarization was further implemented by employing TEC-168S. At the end, a smooth surface with an RMS surface roughness of 5.5 nm was obtained in 20 min (Fig. 13), and the average MRR was 1.7 μm/min. The machining efficiency was increased by 150% compared with that using TEC-168S only. Thus, the good surface was well preprocessed for subsequent machining.

5 Conclusions

A high-efficiency polishing approach for KDP crystal was developed to avoid surface contamination and solve the inefficiency of previous water-dissolution polishing techniques. TAWF was used for controllable deliquescence without any chemical impurity. The product of deliquescence was then removed by a polishing pad to implement surface planarization. The mechanism of TAWF polishing was studied, and a special device was built to polish the KDP crystal. The relationship between RH and polishing performance was investigated, and the effects of polishing pressure and revolution rate on surface planarization were analyzed. In addition, the optimization of the polishing pads and its application were also performed. The main conclusions can be drawn as follows:

1) Uniform dispersion of liquid water is implemented by utilizing the two-phase structure of the TAWF. The amount of moisture absorbed by the KDP crystal is regulated by changing the supply rate of the TAWF, and thus the controllable deliquescence can be achieved.

2) Improving the polishing performance with increasing RH is theoretically feasible. However, the precise control of RH is extremely difficult during the TAWF polishing process. Once RH fluctuates, controllable deliquescence can easily be disrupted and leads to the formation of corrosion structures.

3) In TAWF polishing, material removal is mainly contributed by the synergistic effect of deliquescence and

Table 2 Parameters of composite TAWF polishing process

Polishing stage	Polishing pad	Polishing pressure/kPa	Revolution rate/(r·min^{-1})	MF_{mwp} /(mg·min^{-1})	Rotation rate/(r·min^{-1})	Polishing time/min	Preprocessing method	Relative humidity/%
1st	IC-1000	16	24	200	62	15	Lapping (3000 Grit)	⩽15
2nd	TEC-168S	8	13	150	200	5	N/A	⩽15

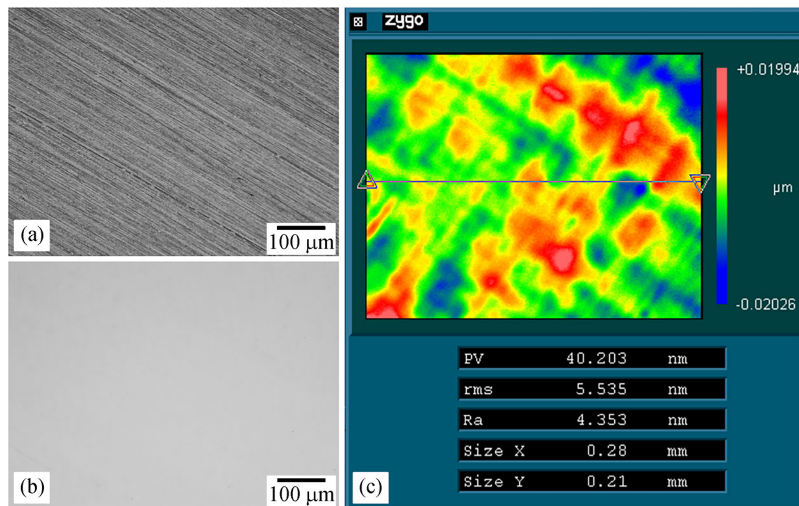

Fig. 13 Surface of KDP crystal obtained through composite TAWF polishing process. Surface topography (a) before and (b) after polishing; (c) surface profile after polishing.

the polishing pad. No effective material removal for KDP crystal without deliquescence can be performed merely by the polishing pad.

4) Excessive polishing pressure and revolution rate degrade the polishing performance and substantially reduce the life of the polishing pad.

5) The machining efficiency was increased by 150% through the composite process of TAWF polishing using IC-1000 and TEC-168S compared with that using TEC-168S only, and a smooth surface with an RMS surface roughness of 5.5 nm was obtained. Thus, a good surface was well preprocessed for the subsequent machining process.

Acknowledgements The authors would like to appreciate the financial support from the National Natural Science Foundation of China (Grant Nos. 51135002 and 51621064).

Open Access This article is licensed under Creative Commons Attribution 4.0 International License, which permits use, sharing, adaptation, distribution, and reproduction in any medium or format, as long as appropriate credit is given to the original author(s) and the source, a link is provided to the Creative Commons license, and any changes made are indicated.

Images or other third-party materials in this article are included in the article's Creative Commons license, unless indicated otherwise in a credit line to the material. If material is not included in the article's Creative Commons license and your intended use is not permitted by statutory regulation or exceeds the permitted use, you will need to obtain permission directly from the copyright holder.

To view a copy of this license, visit http://creativecommons.org/licenses/by/4.0/.

References

1. Dmitriev V G, Gurzadyan G G, Nikogosyan D N. Handbook of Nonlinear Optical Crystals. 3rd ed. Berlin: Springer, 1999
2. Nikogosyan D N. Nonlinear Optical Crystals: A Complete Survey. New York: Springer, 2005
3. Rolle J, Berge L, Duchateau G, et al. Filamentation of ultrashort laser pulses in silica glass and KDP crystals: A comparative study. Physical Review A, 2014, 90(2): 023834
4. Campbell J H, Hawley-Fedder R A, Stolz C J, et al. NIF optical materials and fabrication technologies: An overview. Proceedings of the Society for Photo-Instrumentation Engineers, 2004, 5341: 84–101
5. Hawley-Fedder R A, Geraghty P, Locke S N, et al. NIF Pockels cell and frequency conversion crystals. Proceedings of the Society for Photo-Instrumentation Engineers, 2004, 5341: 121–126
6. Kucheyev S O, Siekhaus W J, Land T A, et al. Mechanical response of $KD_{2x}H_{2(1-x)}PO_4$ crystals during nanoindentation. Applied Physics Letters, 2004, 84(13): 2274–2276
7. Liu Z Y, Gao H, Guo D M. A novel approach of precision polishing for KDP crystal based on the reversal growth property. Precision Engineering, 2018, 53: 1–8
8. Namba Y, Katagiri M, Nakatsuka M. Single point diamond turning of KDP inorganic nonlinear optical crystals for laser fusion. Journal of the Japan Society of Precision Engineering, 1998, 64(10): 1487–1491
9. Tie G P, Guan C L. Study on formation mechanism of periodic ripple on finished KDP crystal in cutting process. Proceedings of the Society for Photo-Instrumentation Engineers, 2015, 95241V
10. Tie G P, Dai Y F, Guan C L, et al. Research on subsurface defects of potassium dihydrogen phosphate crystals fabricated by single point diamond turning technique. Optical Engineering, 2013, 52(3): 033401
11. Zhang F H, Wang S F, An C H, et al. Full-band error control and crack-free surface fabrication techniques for ultra-precision fly cutting of large-aperture KDP crystals. Frontiers of Mechanical Engineering, 2017, 12(2): 193–202
12. Menapace J A, Ehrmann P R, Bickel R C. Magnetorheological

finishing (MRF) of potassium dihydrogen phosphate (KDP) crystals: Nonaqueous fluids development, optical finish, and laser damage performance at 1064 nm and 532 nm. Proceedings of the Society for Photo-Instrumentation Engineers, 2009, 7504: 750414

13. Yin Y H, Zhang Y F, Dai Y F, et al. Novel magneto-rheological finishing process of KDP crystal by controlling fluid-crystal temperature difference to restrain deliquescence. CIRP Annals–Manufacturing Technology, 2018, 67(1): 587–590
14. Ji F, Xu M, Wang C, et al. The magnetorheological finishing (MRF) of potassium dihydrogen phosphate (KDP) crystal with Fe_3O_4 nanoparticles. Nanoscale Research Letters, 2016, 11(1): 79
15. Ji F, Xu M, Wang B R, et al. Preparation of methoxyl poly(ethylene glycol) (MPEG)-coated carbonyl iron particles (CIPs) and their application in potassium dihydrogen phosphate (KDP) magnetorheological finishing (MRF). Applied Surface Science, 2015, 353: 723–727
16. Chen S S, Li S Y, Peng X Q, et al. Research of polishing process to control the iron contamination on the magnetorheological finished KDP crystal surface. Applied Optics, 2015, 54(6): 1478–1484
17. Li F R, Xie X H, Tie G P, et al. Research on temperature field of KDP crystal under ion beam cleaning. Applied Optics, 2016, 55(18): 4888–4894
18. Li F R, Xie X H, Tie G P, et al. Figuring process of potassium dihydrogen phosphate crystal using ion beam figuring technology. Applied Optics, 2017, 56(25): 7130–7137
19. Gao H, Wang X, Teng X J, et al. Micro water dissolution machining principle and its application in ultra-precision processing of KDP optical crystal. Science China. Technological Sciences, 2015, 58(11): 1877–1883
20. Gao H, Wang X, Guo D M, et al. Research progress on ultra-precision machining technologies for soft-brittle crystal materials. Frontiers of Mechanical Engineering, 2017, 12(1): 77–88
21. Gao H, Wang B L, Guo D M, et al. Experimental study on abrasive-free polishing for KDP crystal. Journal of the Electrochemical Society, 2010, 157(9): 853–586
22. Wang B L, Li Y Z, Gao H. Water-in-oil dispersion for KH_2PO_4 (KDP) crystal CMP. Journal of Dispersion Science and Technology, 2010, 31(12): 1611–1617
23. Wang X, Gao H, Chen Y C, et al. A water dissolution method for removing micro-waviness caused by SPDT process on KDP crystals. International Journal of Advanced Manufacturing Technology, 2016, 85(5–8): 1347–1360
24. Dong H, Wang L L, Gao W, et al. KDP aqueous solution-in-oil microemulsion for ultra-precision chemical-mechanical polishing of KDP crystal. Materials (Basel), 2017, 10(3): 271
25. Zhang F H, Guo S L, Zhang Y, et al. Effect of several processing parameters on material removal ratio in the deliquescent polishing of KDP crystals. Proceedings of the Society for Photo-Instrumentation Engineers, 2009, 7282: 728227
26. Lote D A, Vinod V, Patwardhan A W. Computational fluid dynamics simulations of the air–water two-phase vertically upward bubbly flow in pipes. Industrial & Engineering Chemistry Research, 2018, 57(31): 10609–10627
27. Zhang C B, Xia K L, Xu K Y, et al. Two-phase fluid modeling of magnetic drug targeting in a permeable microvessel implanted with a toroidal permanent magnetic stent. Journal of Fluids Engineering–Transactions of the ASME, 2019, 141(8): 081301
28. Gao H, Song C P, Guo D M. Principle of ultra precision polishing with micro water mist for KDP/DKDP crystals. International Journal of Nanomanufacturing, 2015, 11(3–4): 150–160
29. Jimmy B, Kentish S, Grieser F, et al. Ultrasonic nebulization in aqueous solutions and the role of interfacial adsorption dynamics in surfactant enrichment. Langmuir, 2008, 24(18): 10133–10137
30. Liu Z Y, Gao H, Guo D M. Polishing technique for KDP crystal based on two-phase air–water fluid. Precision Engineering, 2019, 56: 404–411